



Mechanism investigation on the enhanced and selective photoelectrochemical oxidation of atrazine on molecular imprinted mesoporous TiO₂



Huijie Shi, Yingling Wang, Chunjing Tang, Weikang Wang, Meichuan Liu, Guohua Zhao*

School of Chemical Science and Engineering, and Shanghai Key Lab of Chemical Assessment and Sustainability, Tongji University, 1239 Siping Road, Shanghai, 200092, China

ARTICLE INFO

Keywords:
Selective photoelectrochemical oxidation
Molecular imprint
Mesoporous TiO₂
Atrazine

ABSTRACT

In this work, enhanced and selective photoelectrochemical (PEC) oxidation of atrazine was realized on molecular imprinted mesoporous TiO₂ (MI-meso-TiO₂). The investigation revealed that, for one hand, the surface MI sites could function as surface defects for accelerating the separation of photogenerated holes and electrons, leading to enhanced generation of hydroxyl radicals. For the other hand, the MI sites showed enhanced binding affinity toward atrazine, resulted from the formation of multiple hydrogen bonds and halogen bonds etc., which was testified by in situ ATR-FTIR spectra. It led to the enhanced adsorption and improved local concentration of atrazine on the electrode surface. Both the two factors contributed to the improved PEC oxidation activity for atrazine on MI-meso-TiO₂ compared with that on meso-TiO₂. Moreover, the high binding affinity between MI sites and atrazine resulted in the selective recognition ability toward atrazine in the presence of the coexisting pollutants, so that selective PEC oxidation of atrazine in complex polluted water samples was successfully achieved on MI-meso-TiO₂ with the apparent rate constant of 0.25 h⁻¹, whereas that on meso-TiO₂ was only 0.08 h⁻¹. This work provided something new for explaining the selective and enhanced PEC performance on molecular imprinting catalyst.

1. Introduction

Nowadays, the contaminants in the environment presents the characteristics that pollutants of high toxicity and low concentration always coexist with that of low toxicity and high concentration. The typical high toxicity contaminants include pharmaceuticals, pesticides, industrial organic pollutant and etc [1]. They have posed significant risk to human health although with low concentration. In conventional water treatment systems, these high toxicity contaminants are mostly partially removed owing to the low concentration and poor biodegradability [2]. In order to achieve complete detoxification and purification, it is highly desirable to combine the conventional biological treatment with an efficient and selective advanced oxidation technique to constitute a more efficient and cost-effective process for complex, multi-pollutant wastewater treatment, i.e. to remove these high-toxicity and low-concentration pollutants selectively before or after subjected to conventional water treatment system.

Photoelectrochemical (PEC) oxidation has attracted growing attention as a kind of advanced oxidation process (AOP) in waste water

treatment [3–5], which inherits the advantages of photocatalytic (PC) oxidation, such as high efficiency, environmental friendliness, cost-effectiveness and etc. By adding a bias potential on the electrode, the efficiency of the PC oxidation will be further improved owing to the accelerated separation of the photo-generated electrons and holes. PEC oxidation is quite promising in removing contaminants with low concentration in the water [6,7]. By adsorption on the PEC electrode, the contaminants of low-concentration will be enriched on the electrode surface, leading to an enhanced oxidation efficiency. However, to achieve the selective removal of the target contaminant in PEC oxidation is still challenging, because the active oxidizing species in PEC process are primary hydroxyl radicals, which can attack any organic substances subjected to the PEC treatment [8].

We notice that the enzyme catalysis in the nature has the advantages of high efficiency and selectivity. In the enzyme catalytic process, the target substrates are selectively adsorbed and activated on the active sites of the enzyme, and then transformed efficiently. We can find that there is similarity between the PEC reaction and the enzymatic reaction. In both the process, the substrates are adsorbed firstly on the

* Corresponding author.

E-mail address: g.zhao@tongji.edu.cn (G. Zhao).

catalytic platform before the catalytic reaction occurs. Therefore, if active sites with selective recognition ability can be fabricated on the photo-electrode, so that the target contaminant can be adsorbed selectively in the active sites, selective PEC oxidation of the contaminant will be achieved by mimicking the enzyme catalytic reaction.

Molecular imprinting technique (MIT) is a kind of promising approaches for creating artificial molecular recognition (MI) sites on the matrix utilizing the target molecules as template, which were complementary to the template molecules in shape, size and functional groups distribution [9–11]. By fabricating MI sites on the catalyst surface, not only PC or PEC selectivity towards the target molecules can be obtained, but also the oxidation efficiency is improved, which is mostly ascribed to the enhanced adsorption of the targets on the MI sites [12–14]. However, the intrinsic reasons for the enhanced oxidation efficiency is not fully addressed.

In this work, mesoporous TiO_2 endowed with large specific surface area and open pore channel is chosen as the molecular imprinting matrix owing to its excellent PC activity, chemical stability and environmental safety [15,16]. The large surface area can not only improve the PEC oxidation ability efficiently, but also is beneficial for introducing more MI sites, leading to enhanced specific adsorption capability [17]. Meanwhile, the open pore channel makes the MI sites fabricated on the pore walls more accessible, and in favor of the fast mass transport of the reactants and products. Atrazine (Fig. S1) is chosen as a research model because it is a pesticide representative of a class of dangerous contaminant in water as stated by the World Health Organization [1,18]. It has attracted much interest owing to its wide application in agriculture, high toxicity and slow biodegradation in the environment [19]. Many advanced oxidation process (AOP) have been developed for atrazine removal including electrochemical (EC) oxidation [20], PC oxidation [21], Fenton oxidation [22] and etc. But the selective removal of atrazine is rarely discussed.

Herein, the molecular imprinted mesoporous TiO_2 photoanode (MI-meso- TiO_2) was fabricated employing an evaporation induced self-assembly (EISA) method with atrazine as MI template. The enhanced PEC oxidation of atrazine on MI-meso- TiO_2 was investigated in detail by comparison with that on meso- TiO_2 . The intrinsic reasons for the improved PEC oxidation efficiency was discussed based on the enhanced binding affinity between atrazine and MI-meso- TiO_2 compared with meso- TiO_2 , as well as the enlarged local concentration on electrode surface brought about by MI sites. What's more, the efficient charge transfers in MI-meso- TiO_2 was also investigated by time-resolved fluorescence emission decay spectra, and proved by the measurement of hydroxyl radicals generated in PEC process. MI-meso- TiO_2 was then applied in the selective PEC oxidation of atrazine in both mono- and complex systems in order to evaluate the recognition performance toward the target pollutant. The mechanism for the PEC selectivity was also discussed. This work provided the insight into the enhanced oxidation efficiency and selectivity in molecular imprinting technique based PEC process, and paved a way to establish the efficient and selective PEC method for treating special pollutant with low concentration and high toxicity in complex environmental water.

2. Experimental

2.1. Materials and apparatus

All the chemicals are commercially available as analytical reagent grade and used as received unless otherwise stated. PESTANAL® analytical standards such as Atrazine-2-hydroxy (HA), Atrazine-desisopropyl (DIA), Atrazine-desethyl (DEA), and Atrazine-desethyl-2-hydroxy (HDEA) were bought from Sigma-Aldrich as control to identify the degradation intermediates by HPLC.

The morphologies and crystal structures of the mesoporous TiO_2 with and without MI sites were characterized by the Field emission scanning electron microscope (FE-SEM, Hitachi S-4800) and high

resolution transmission electron microscope (HR-TEM, JEM 2100). The powder X-ray diffraction (XRD) were measured on a Bruker D8 Advance X-ray diffractometer. The N_2 adsorption-desorption analysis was performed at 77 K using a Micromeritics TriStar 3020 instrument. Prior to the measurement, the samples were degassed at 473 K overnight. The Brunauer-Emmet-Teller (BET) surface area was calculated from the selected N_2 adsorption data within the range of relative pressure from 0.05 to 0.2. The total pore volume (V_t) was determined as the volume of liquid nitrogen adsorbed at a relative pressure of 0.99. The pore size distributions were obtained using the Barrett-Joyne-Halenda (BJH) method from the adsorption branch. UV-vis diffuse reflectance spectra (DRS) were measured on an ultraviolet visible spectroscopy of diffuse reflectance (AvaLight-DHS, Avantes, Netherlands). UV-vis absorption spectra was collected on an Agilent 8453 ultraviolet and visible spectrophotometer. Fourier transform infrared spectra (FT-IR) were collected in the region from 400 to 4000 cm^{-1} at room temperature using a Nicolet 8700 spectroscopy. Raman spectra were recorded using a Raman microscope (inVia reflex, Renishaw, UK) with the excitation source at 532 nm. The fluorescence lifetime was determined with a steady state/transient fluorescence spectrometer (JY Fluorolog-3-Tou, Jobin Yvon Co., France). The excitation wavelength was 340 nm, and the decay curve was monitored at 550 nm.

2.2. Preparation of MI-meso- TiO_2

MI-meso- TiO_2 was prepared by the EISA method combined with MIT. Typically, Pluronic P123 (1.0 g, 0.2 mmol) was dissolved in ethanol (12 g). Then, 62 mg atrazine was added to the solution as MI templates. The mixture was stirred for 30 min to enable the adequate interaction between P123 and atrazine. Afterwards, 25.6 mmol concentrated hydrochloric acid together with 14.12 mmol of tetraethyl orthotitanate (The mole ratio of atrazine/Ti was kept as 2%) were added, which was stirred for another 2 h under ambient conditions. The prepared sols were dip-coated on the cleaned Ti plate with a 6 mm/s withdrawing rate after Ti plate was immersed in the sols for 10 min and dried under ambient conditions for about 24 h. Finally, the electrode was calcined at 450 °C in air for 30 min at a ramping rate of 0.7 °C/min to induce the mesoporous microstructure and remove the MI template. The catalyst loading amount of MI-meso- TiO_2 on the electrode was determined to be 0.18 mg cm^{-2} with three parallel experiments.

Meso- TiO_2 was prepared as control with the same method as described above, except that atrazine was omitted. The loading amount of meso- TiO_2 was also determined to be about 0.19 mg cm^{-2} .

2.3. PEC degradation of atrazine in water samples

PEC oxidation of atrazine was carried out in a cylindrical single-compartment cell equipped with a magnetic stirrer and a jacketed cooler to maintain a constant temperature (such as 25 ± 2 °C). MI-meso- TiO_2 with a working area of 15 cm^2 was used as the anode, a Pt sheet with the same area as the cathode, a saturated calomel electrode (SCE) as the reference electrode, and the gap between the electrodes was about 2 cm. A bias potential of 0.6 V vs. SCE was applied on the working electrode. A 300 W Xe high-pressure short-arc xenon lamp (PLS-SXE300, PerfectLight Technology Co., Ltd. Beijing) equipped with an IR cut-off filter was used as light source. The light intensity was determined to be about 140 mW cm^{-2} . 90 mL of 10 mg L^{-1} atrazine in 0.1 M Na_2SO_4 was added in the cell. Before light irradiation, atrazine was allowed to reach the adsorption-desorption equilibrium on the anode surface in 30 min, and the concentration of atrazine in solution was denoted as C_0 . The sample was monitored and analyzed as a function of time. The concentration of atrazine was determined by high-pressure liquid chromatography (HPLC, Agilent 1260) equipped with an Agilent TC-C18 column (150 mm × 4.6 mm, 5 μm). The mobile phase was the mixed solution of acetonitrile and water (60/40, v/v) with a flow rate of 1 mL/min. The detection wavelength was 220 nm.

One-ml sample was regularly taken and filtered by 0.22 µm membrane filter before HPLC analysis.

Atrazine and its degradation intermediates were analyzed by liquid chromatography-mass spectrometry (LC-MS, Varian 310) with an Agilent C18 column (150 mm × 4.6 mm, 5 µm). The mobile phase was the mixed solution of acetonitrile and water (50/50, v/v) with a flow rate of 0.6 mL/min. The mass spectra were recorded across the range of 50–300 m/z with the positive scan mode. The results were further confirmed by measuring the PESTANAL® analytical standards of the proposed intermediates with HPLC.

2.4. ATR-FTIR spectroscopy investigation on atrazine adsorption on MI-meso-TiO₂

For IR investigation, a self-made attenuated total reflection (ATR) unit was attached on a Nicolet 8700 FTIR spectrometer equipped with an MCT detector. The spectra were recorded by averaging 100 scans at a resolution of 8 cm⁻¹, and represented as -log(R/R₀), where R and R₀ were the single beam spectra corresponding to the samples and the reference.

MI-meso-TiO₂ film was immobilized on the ATR prism (a hemispherical Si prism) by spreading 25 µL of MI-meso-TiO₂ dispersion (100 mg in 0.9 mL ethanol and 0.1 mL wt. 5% Nafion dispersion), and dried in a nitrogen stream. Then, the glass IR cell was assembled by pressing against the pre-coated prism using a Teflon ring. The cell was filled with 0.1 M Na₂SO₄ aqueous solution or 2 ppm atrazine in 0.1 M Na₂SO₄ aqueous solution to measure the reference or sample spectrum, respectively.

3. Results and discussion

3.1. Fabrication and characterization of MI-meso-TiO₂

Scheme 1A illustrated the concept and fabrication process of MI-meso-TiO₂. FT-IR spectra was applied to monitor the fabrication process of MI sites. Here, P123 was employed as the mesoporous template, and atrazine as MI template. In the process of sol-gel, both P123 and atrazine was included in the matrix of TiO₂. As shown in Fig. S2, before calcination, both the characteristic peaks of P123 and atrazine could be found. However, after calcination, the peaks for P123 and atrazine disappeared in the IR spectra except for that of TiO₂, indicating the successful removal of the templates and formation of MI sites of atrazine on the mesoporous TiO₂.

Fig. S3 showed the morphologies of meso-TiO₂ and MI-meso-TiO₂. Obvious porous structures were obtained for both the photo-anodes. The thickness of TiO₂ film on the substrates was about 1.3 µm. The lattice fringes with spacing of 0.35 nm and 0.23 nm could be indexed to the (101) and (112) facet of TiO₂, indicating the formation of anatase phase TiO₂. The crystalline phase of meso-TiO₂ and MI-meso-TiO₂ was further confirmed by the wide-angle XRD (Fig. 1A). The 2θ values at 25.3°, 37.8°, 48.0°, 53.9°, 55.1°, 62.7°, 68.8°, 70.3°, and 75.0° agreed well with the (101), (004), (200), (105), (211), (204), (116), (220) and (215) planes of the anatase TiO₂ (PDF#21-1272).

To verify the mesoporous structures of the photo-anodes, small-angle X-ray diffraction (SAXRD) patterns were recorded and shown in Fig. 1B. The typical low-angle reflections at 2θ = 0.56° indicated the presence of uniform mesoporous structures in both meso-TiO₂ and MI-meso-TiO₂ [23]. N₂ adsorption-desorption isotherms of both meso-TiO₂ and MI-meso-TiO₂ (Fig. 1C) presented the type-IV curves which further reflected the presence of mesopores. The pore size distribution curves illustrated the narrow pore sizes distribution, and the average pore sizes obtained by BJH method were 4.8 nm for meso-TiO₂ and 4.7 nm for MI-meso-TiO₂. The BET surface areas of meso-TiO₂ and MI-meso-TiO₂ were determined as 83 and 89 m²/g respectively. The above results suggested that the introduction of MI sites on the meso-TiO₂ not only did not alter the morphologies and crystalline phase of the material, but also the

influence on the mesoporous structure was negligible.

The successful fabrication of MI sites on MI-meso-TiO₂ was testified by the enhanced adsorption capacity of atrazine on MI-meso-TiO₂, which was determined to be 4.48 mg/g by the static adsorption experiment, and it was approximately 1.8 times that on meso-TiO₂. This result was also consistent with the improved PEC responses of atrazine on MI-meso-TiO₂. As shown in Table 1, ΔI/I₀ was used to represent the PEC responses, where ΔI was the photocurrent increment before and after addition of the contaminates, and I₀ was the photocurrent in 0.1 M Na₂SO₄ without contaminates. The photocurrent response of atrazine ΔI/I₀(atrazine) was about 12.1% on MI-meso-TiO₂, which was about 2.9 times that on meso-TiO₂.

3.2. Mechanism on the enhanced PEC oxidation of atrazine on MI-meso-TiO₂

As indicated above, the introduction of MI sites on MI-meso-TiO₂ would lead to the enhanced atrazine adsorption and PEC oxidation on MI-meso-TiO₂. Here, PEC removal of atrazine on MI-meso-TiO₂ and meso-TiO₂ was performed in 0.1 M Na₂SO₄. The average results of three parallel experiments were shown in Fig. 2A. With 10 ppm as the initial concentration, atrazine was removed for about 93.9% in 10 h on MI-meso-TiO₂, whereas that on meso-TiO₂ was 69.8%. An improvement of about 34.5% for atrazine removal further proved that by fabricating MI sites on photo-anode, the PEC catalytic efficiency of MI-meso-TiO₂ was significantly enhanced. The PEC oxidation efficiency of atrazine on MI-meso-TiO₂ was also compared with that of photocatalytic and electrochemical oxidation method. As shown in Fig. 2C, the application of bias potential could efficiently improve the PEC oxidation efficiency by accelerated the separation of photo-generated electrons and holes [24].

The kinetics plots were provided in Fig. 2B. The PEC oxidation of atrazine on both MI-meso-TiO₂ and meso-TiO₂ followed a pseudo-first-order reaction in kinetics as given below:

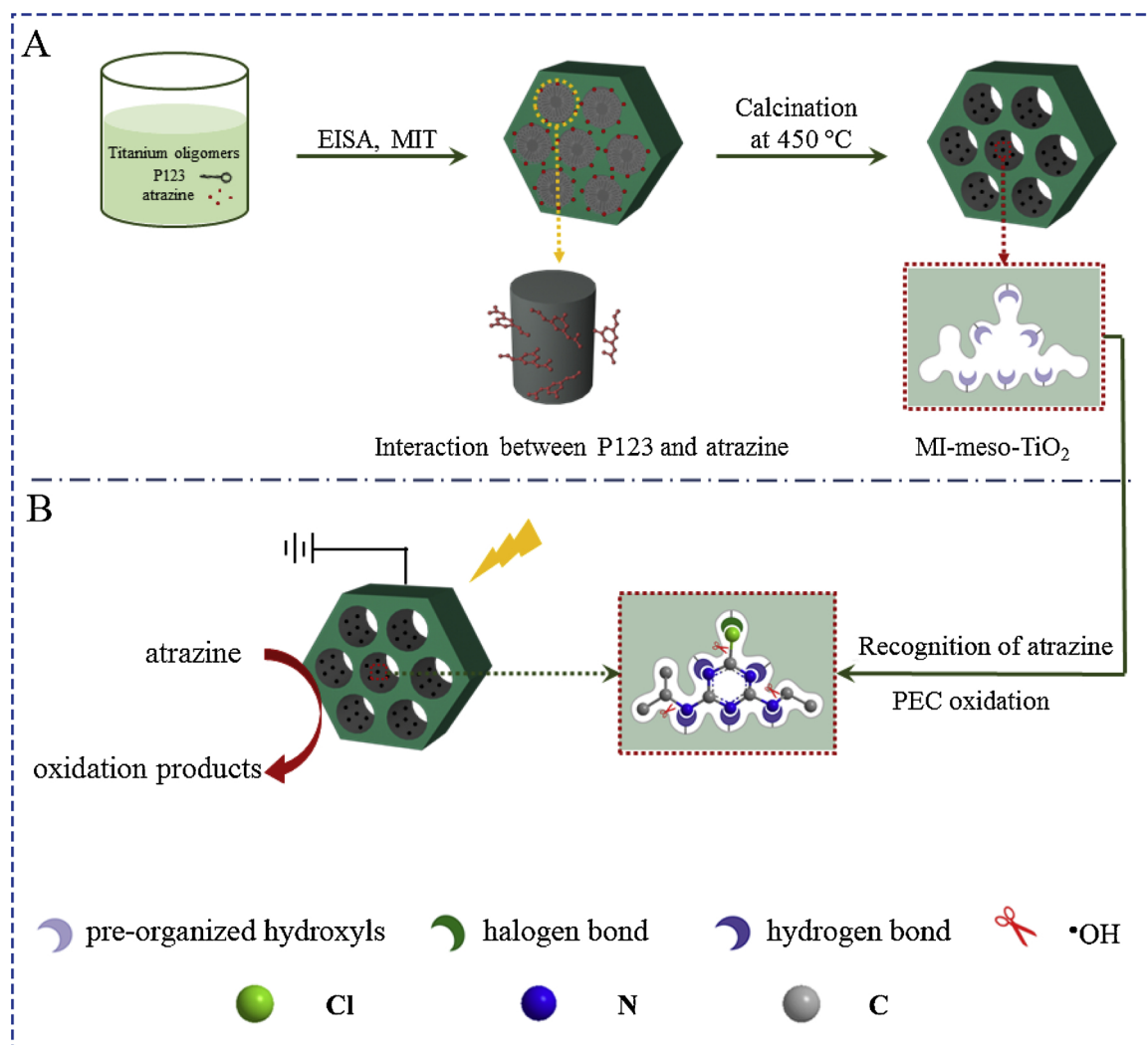
$$\ln \frac{c_t}{c_0} = -k_{app} t + y \quad (1)$$

Where, c₀ and c_t represented the initial concentration of atrazine and the concentration under PEC oxidation at time t (hour), k_{app} was the apparent rate constant of the pseudo-first-order reaction, and y was a constant. The k_{app} of atrazine oxidation on MI-meso-TiO₂ was achieved as 0.28 h⁻¹, whereas that on meso-TiO₂ was 0.12 h⁻¹. An imprinting factor for atrazine oxidation was defined for elaborating the contribution of MI sites in enhancing the reaction kinetics.

$$F_{kinetic} = \frac{k_{app}(MI-meso-TiO_2)}{k_{app}(meso-TiO_2)} \quad (2)$$

F_{kinetic} of 2.3 confirmed that the PEC oxidation kinetics of atrazine was accelerated by fabricating MI sites on MI-meso-TiO₂.

In order to elucidate the intrinsic reasons for the enhanced atrazine PEC oxidation efficiency, the charge carrier dynamics of meso-TiO₂ before and after fabricating MI sites were firstly studied by time-resolved fluorescence emission decay spectra. As shown in Fig. 3A, the average fluorescence lifetimes for meso-TiO₂ and MI-meso-TiO₂ were obtained as 0.58 and 0.51 ns respectively. The relatively shorter fluorescence lifetime of MI-meso-TiO₂ was attributed to the introduction of MI sites on the electrode surface, which may function as trap sites for charge carriers like surface defects [25]. However, it may also indicate that when contacting with water or hydroxyls, the MI sites would accelerate the transfer of photo-generated holes to the catalyst surface, and make more hydroxyl radicals to be generated. This speculation was confirmed by quantification of hydroxyl radicals produced on MI-meso-TiO₂ and meso-TiO₂. Terephthalic acid was used as probe molecule to capture the generated ·OH, and the fluorescence which was proportional to the amount of ·OH was measured [26]. As shown in Fig. 3B, the amount of ·OH, represented by the fluorescence intensity, increased linearly with the irradiation time on both MI-meso-TiO₂ and meso-TiO₂.



Scheme 1. Fabrication process of MI-meso-TiO₂ (A) and the enhanced and selective PEC catalytic behavior of MI-meso-TiO₂ (B).

However, •OH was generated more quickly and efficiently on MI-meso-TiO₂. Consequently, it would lead to the improved efficiency in PEC oxidation of atrazine.

Since that the efficient binding and adsorption of substrates on the catalyst surface was crucial in improving the PEC oxidation ability, the interaction between atrazine and MI-meso-TiO₂ was also investigated. The binding mode between atrazine and MI-meso-TiO₂ was detected by *in situ* ATR-FTIR spectroscopy. As illustrated in Fig. 4A, with time increasing, the characteristic peaks of atrazine increased accordingly. It indicated more and more atrazine was adsorbed on the surface of MI-meso-TiO₂. The adsorption reached equilibrium in about 25 min. The broad absorption around 3380 cm⁻¹ suggested hydrogen bonding was formed between atrazine and the surface hydroxyl groups of MI-meso-TiO₂ [27]. Meanwhile, the IR spectra of pure atrazine was also recorded for comparison by dropping atrazine chloroform solution on the KBr pellet. As shown, the characteristic absorption peaks at 806 and 772 cm⁻¹ were attributed to the C-Cl vibrations. Upon adsorption on MI-meso-TiO₂, the two peaks merged together to form a broad absorption, and red shifted to about 702 cm⁻¹, manifesting the formation of halogen bonding between the chlorine atom of atrazine and hydroxyl groups of MI-meso-TiO₂. The absorption peaks of atrazine at 1622 and 1542 cm⁻¹ were due to the deformation of triazine ring in plane [28]. Interestingly, we could find that the absorption intensity of the two peaks changed inversely when adsorbed on MI-meso-TiO₂. It may indicated the interaction between the triazine ring of atrazine and the MI-

meso-TiO₂ surface, such as d-π bonding [29]. Similar but less obvious phenomenon was also found in atrazine adsorption on meso-TiO₂.

As known, there were plenty of hydroxyls on the surface of TiO₂. By fabrication of MI sites, hydroxyls distributed complementary to the functional groups of atrazine would be formed around the MI sites [8]. When atrazine was rebounded to the MI sites, multiple hydrogen bonds and halogen bonds would be reformed between atrazine and the pre-organized hydroxyls on MI-meso-TiO₂ (Scheme 1B). It was worth noting that similar kinds of interaction could also be formed between atrazine and meso-TiO₂. However, lacking the pre-organized hydroxyls on meso-TiO₂, the binding affinity between atrazine and meso-TiO₂ was relatively weaker without the synergistic effect of multiple intermolecular interactions. The enhanced binding affinity between atrazine and MI-meso-TiO₂ was further verified by the UV-vis DRS method. The UV-vis DRS spectra of MI-meso-TiO₂ before and after adsorption of atrazine were collected and compared with that of meso-TiO₂. The samples was prepared by mixing 10 mg/L atrazine with MI-meso-TiO₂ or meso-TiO₂, centrifugalized, washed with water completely to remove the loosely attached atrazine, and dried under 60 °C under vacuum for 24 h. By strictly keeping the condition the same, the comparison of different binding ability on MI-meso-TiO₂ and meso-TiO₂ was rational. As shown in Fig. 4B and S1, both TiO₂ and atrazine exhibited no measurable absorption in the visible light region. However, after adsorption of atrazine, obvious visible light absorption was observed on MI-meso-TiO₂, whereas no similar phenomenon was obtained on meso-

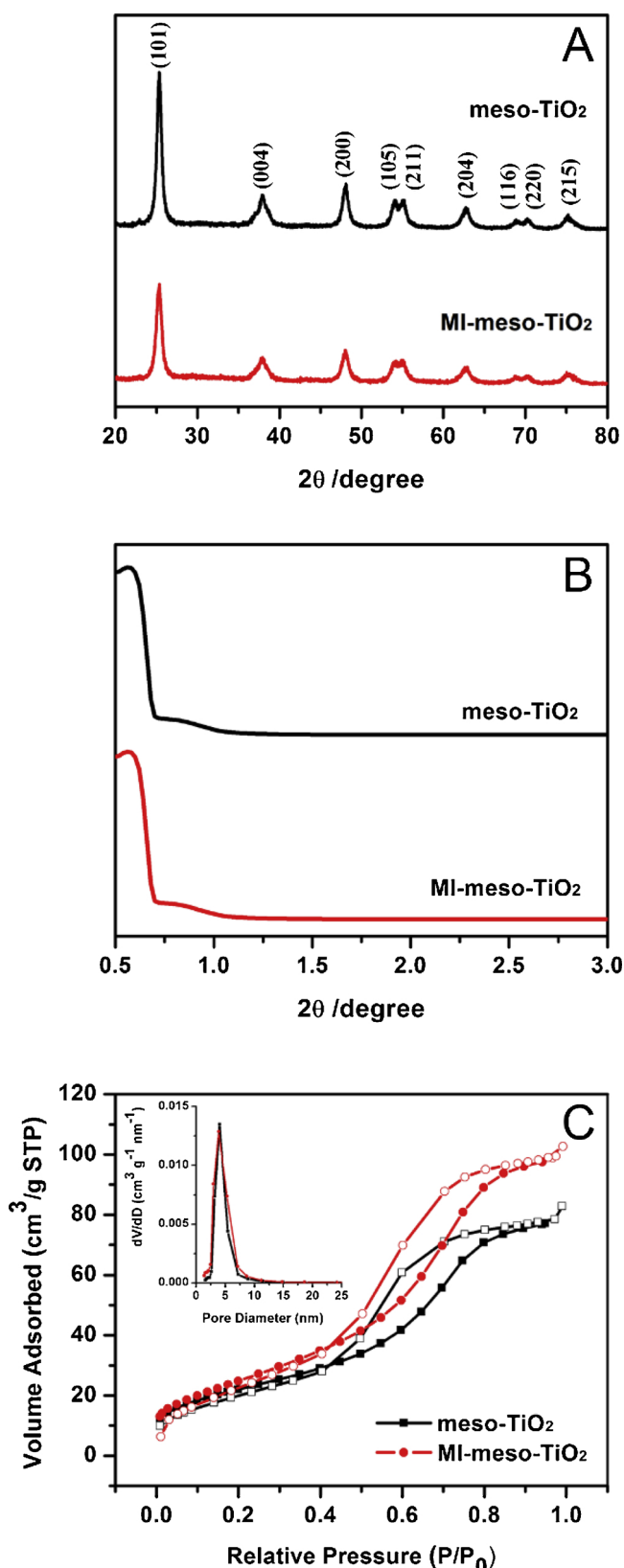


Fig. 1. (A) Wide angle XRD, (B) small angle XRD, (C) N₂ adsorption-desorption isotherms measured at 77 K (inset is the pore size distributions from the adsorption branches through the BJH method) of MI-meso-TiO₂ and meso-TiO₂.

Table 1

Photocurrent responses of different contaminates on MI-meso-TiO₂ and meso-TiO₂.

Photocurrent responses	MI-meso-TiO ₂	Meso-TiO ₂
$\Delta I/I_0$ (atrazine)	12.1%	4.2%
$\Delta I/I_0$ (hexazinone)	7.1%	5.3%
$\Delta I/I_0$ (2,4-D)	6.2%	6.4%
α_{MI} atrazine	2.88	
α_{MI} hexazinone	1.34	
α_{MI} 2,4-D	0.97	

TiO₂. According to the literature, the improved light absorption in visible region could be ascribed to the multiple intermolecular interaction between atrazine and MI-meso-TiO₂, including the formation of hydrogen bonds and halogen bonds between the pre-organized hydroxyls and atrazine, as well as the d-π interaction between TiO₂ surface and the triazine ring [30,31]. The enhanced visible light absorption on MI-meso-TiO₂ indicated that the binding affinity between atrazine and MI-meso-TiO₂ was much stronger than that of meso-TiO₂ owing to the introduction of MI sites. Consequently, it would shift the adsorption equilibrium positively when atrazine was adsorbed on MI-meso-TiO₂, resulted in the improved atrazine adsorption on MI-meso-TiO₂ as indicated above. The enlarged local concentration of atrazine on MI-meso-TiO₂ was beneficial to the PEC oxidation, resulted in enhanced oxidation efficiency and kinetics. It was more important that by forming hydrogen bonds or halogen bonds between the MI sites and atrazine, the bond length of atrazine associated would be increased and the bond energy decreased, so that it was more easily to be attacked by the active oxidizing species, such as hydroxyl radicals.

The above investigation well explained the enhanced PEC current response and oxidation of atrazine on MI-meso-TiO₂. For one hand, by introduction of MI sites, the PEC oxidation activity of MI-meso-TiO₂ was improved by accelerating the charge transfer to the catalyst surface and generating more hydroxyl radicals. For the other hand, MI sites significantly improved the binding affinity between atrazine and the catalyst surface by forming multiple supramolecular interactions, which was beneficial for atrazine adsorption and the attacking by hydroxyls radicals. All these factors contributed to the enhanced PEC oxidation efficiency and fast oxidation kinetics of atrazine on MI-meso-TiO₂.

Finally, the apparent activation energy was determined to elaborate the overall activation effect of MI sites in PEC oxidation process [32,33]. Temperature dependent PEC oxidation of atrazine was carried out on MI-meso-TiO₂ and meso-TiO₂ respectively. As shown in Fig. 5A and B, the apparent rate constant k_{app} increased accordingly with the temperature on both the photo-anodes. Fig. 5C and D showed the plot of ln k_{app} as a function of 1/T. According to the Arrhenius equation:

$$\ln k_{\text{app}} = \frac{-E_a}{R} \frac{1}{T} + \ln A \quad (3)$$

Where A was the frequency factor (h⁻¹), T the temperature (K) and R the gas constant. The apparent activation energy for atrazine oxidation on MI-meso-TiO₂ was obtained as 6.85 kJ mol⁻¹ according to the slopes of the straight lines, whereas that on meso-TiO₂ was 14.84 kJ mol⁻¹. The reduced activation energy further confirmed that the PEC catalytic effect of MI-meso-TiO₂ on atrazine oxidation was more efficient than that of meso-TiO₂, owing to the introduction of MI sites.

3.3. Selective PEC oxidation of atrazine on MI-meso-TiO₂

In this work, MI sites were introduced not only to improve the PEC oxidation efficiency, but also to obtain the selective recognition ability to the target contaminant. So selective recognition ability of MI-meso-TiO₂ towards atrazine in PEC oxidation was also investigated in depth. Hexazinone, which had similar molecular structure with atrazine, and

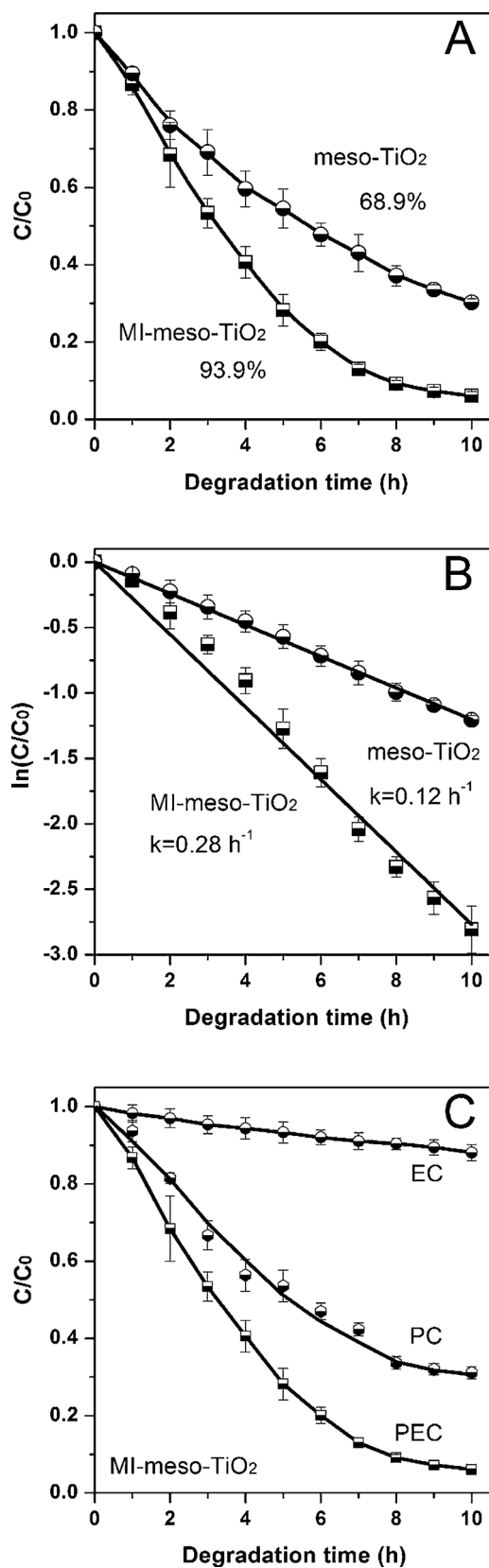


Fig. 2. (A) PEC atrazine removal and (B) atrazine oxidation kinetics on MI-meso-TiO₂ and meso-TiO₂; (C) comparison of the PC, EC and PEC oxidation of atrazine on MI-meso-TiO₂.

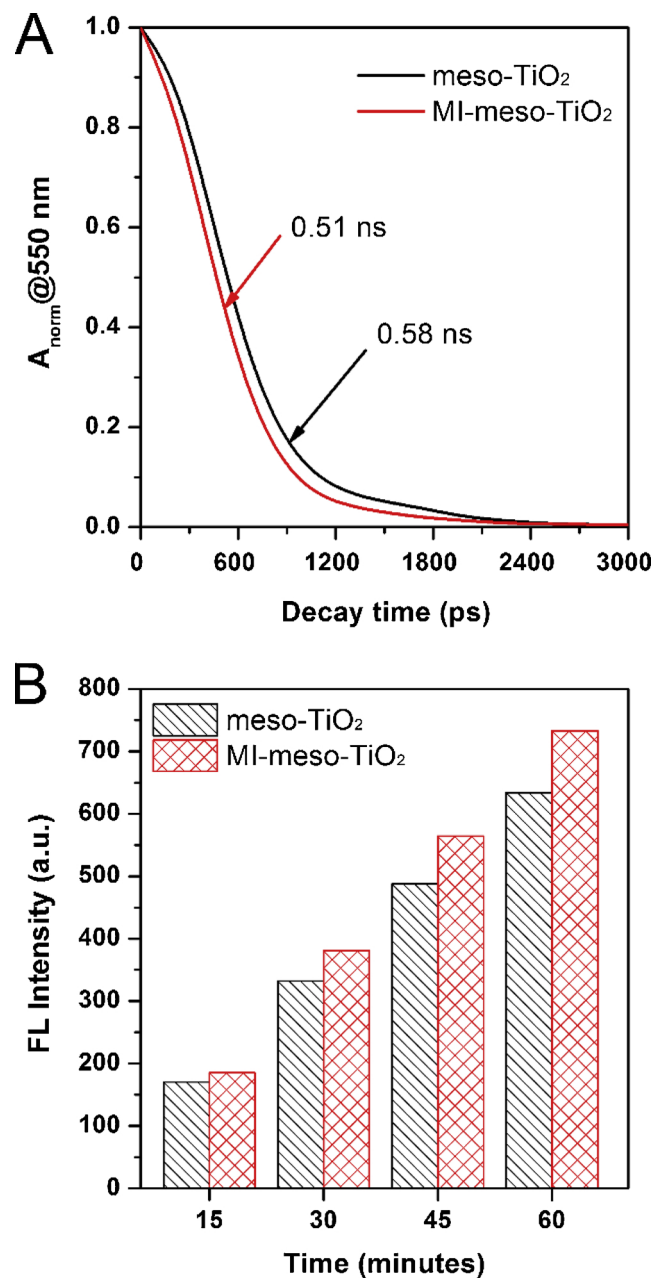


Fig. 3. (A) Time-resolved fluorescence emission decay spectra of meso-TiO₂ and MI-meso-TiO₂; (B) the quantification of hydroxyl radicals produced on MI-meso-TiO₂ and meso-TiO₂.

2,4-dichlorophenoxyacetic acid (2,4-D), which was a typical pesticide commonly present in the water, were selected for comparison [34,35].

The photocurrent responses of MI-meso-TiO₂ and meso-TiO₂ in the presence of atrazine, hexazinone and 2,4-D individually was firstly recorded and the results were summarized in Table 1. As shown, the PEC response of atrazine on meso-TiO₂ was slightly smaller compared with that of hexazinone and 2,4-D, indicating that atrazine was relatively harder to be oxidized. However, the PEC response of atrazine $\Delta I/I_0(\text{atrazine})$ significantly increased to 12.1% on MI-meso-TiO₂, nearly three times ($\alpha_{\text{MI, atrazine}}$) that on meso-TiO₂, whereas the increment of hexazinone was only about 34% ($\alpha_{\text{MI, hexazinone}}$), and that of 2,4-D ($\alpha_{\text{MI, 2,4-D}}$) was nearly the same. These results indicated the great selective enhancement effect of MI sites in the PEC oxidation of atrazine compared with other contaminants. Even hexazinone, which has similar structure with atrazine, the enhancement degree was relatively lower, suggesting the excellent recognition ability of MI sites toward atrazine.

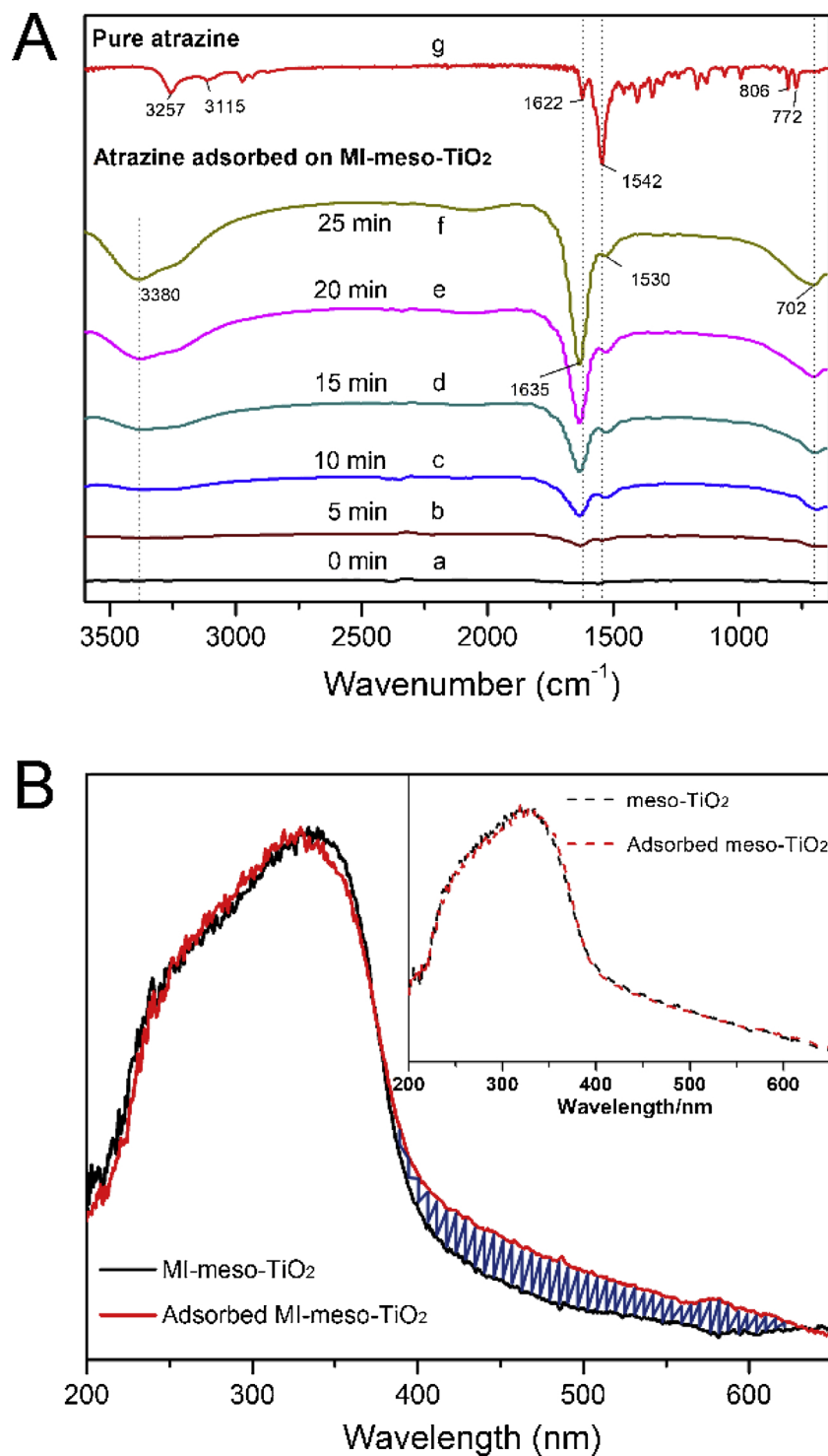


Fig. 4. (A) In situ ATR-FTIR and (B) UV-vis DRS investigation on the interaction between atrazine and MI-meso-TiO₂ surface.

To further study the selectivity of PEC oxidation, PEC oxidation removal of atrazine, hexazinone and 2,4-D with the same concentration was carried out on MI-meso-TiO₂ and meso-TiO₂, respectively. Especially, PEC oxidation of atrazine-desisopropyl (DIA), one of the oxidation intermediate of atrazine, was also conducted to make the comparison more reliable. As shown in Fig. 6A, all the processes followed the pseudo-first-order kinetics. On meso-TiO₂, the PEC oxidation rate constants for atrazine, hexazinone, DIA and 2,4-D were 0.12, 0.17, 0.07 and 0.21 h⁻¹, whereas that on MI-meso-TiO₂ were 0.28, 0.19, 0.08 and 0.18 h⁻¹ respectively (Fig. 6B). It further confirmed the selective

recognition ability of MI sites toward atrazine. Here, a selective factor ($F_{\text{selectivity}}$) was defined to illustrate the recognition ability of MI sites to discriminate different substrates:

$$F_{\text{selectivity}} = \frac{k_{\text{app}}(\text{atrazine})/k_{\text{app}}(\text{interferent}) \text{ on MI-meso-TiO}_2}{k_{\text{app}}(\text{atrazine})/k_{\text{app}}(\text{interferent}) \text{ on meso-TiO}_2} \quad (4)$$

$F_{\text{selectivity(atrazine/2,4-D)}}$ was obtained as 2.72 on MI-meso-TiO₂, indicating the excellent recognition ability of MI sites towards atrazine in PEC oxidation. On the contrary, $F_{\text{selectivity(atrazine/hexazinone)}}$ and $F_{\text{selectivity(atrazine/DIA)}}$ was obtained as 2.09 and 2.04, which was

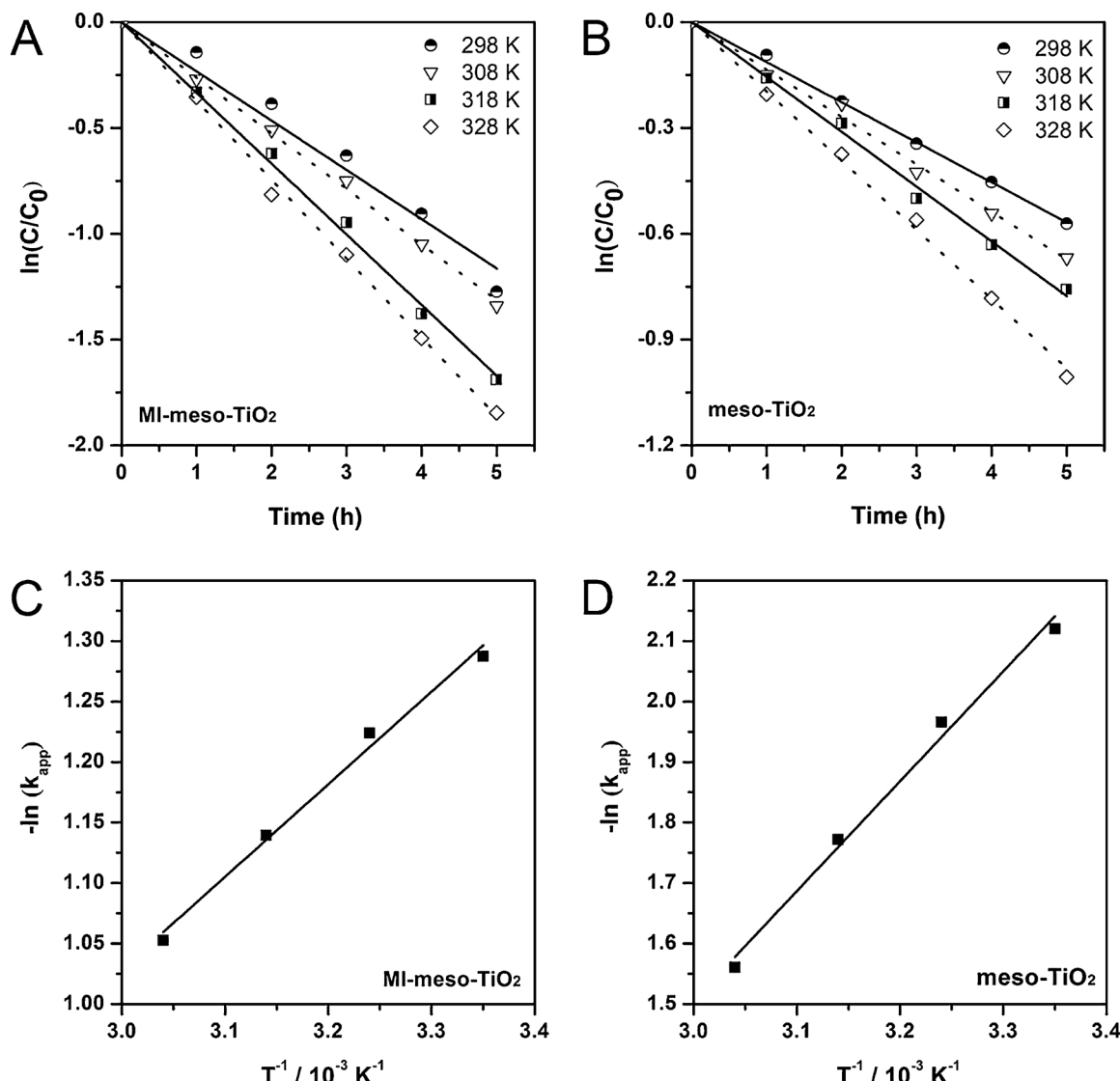


Fig. 5. (A and B) Temperature dependent kinetics plots and (C and D) Arrhenius plots for PEC oxidation of atrazine on MI-meso-TiO₂ and meso-TiO₂.

relatively smaller.

These results could be explained as follow. As discussed above, by introduction of MI sites, strong supramolecular interactions between atrazine and the pre-organized functional groups around MI sites were formed, and led to the selective and enhanced adsorption of atrazine on the surface of MI-meso-TiO₂. On the contrary, the adsorption of 2,4-D, DIA and hexazinone on MI-meso-TiO₂ was much lower, since they could not be recognized and adsorbed in MI sites. This consumption was evidenced by the electrochemical adsorption measurement [36]. The adsorption capacity (Γ) obtained with a chronocoulometric method of atrazine, hexazinone, DIA and 2,4-D on MI-meso-TiO₂ was 4.4×10^{-11} , 1.4×10^{-11} , 2.4×10^{-11} and 1.0×10^{-11} mol·cm⁻² respectively. It was worth noting that compared with 2,4-D, the chemical structure of hexazinone and DIA was similar with atrazine, so it could be recognized and adsorbed on MI-meso-TiO₂ to a certain degree with relative lower binding affinity, resulted in a relatively smaller $F_{\text{selectivity}}(\text{atrazine/hexazinone})$. As known, the major reactive oxidizing species in PEC oxidation process were hydroxyl radicals, whose lifetime was very short (in the range of 10^{-9} s), so the distribution distance of ·OH on the anode surface was also very short (in nanoscale), especially in the present of organics [37]. Therefore, only the contaminants in the vicinity of the surface could be oxidized, especially that adsorbed on the surface. In the PEC oxidation process, atrazine was more easily to be

recognized and adsorbed on the catalyst surface and activated by the supramolecular interaction with MI sites, while the adsorption of hexazinone, DIA and 2,4-D on the surface was not so effective. It led to more efficient PEC oxidation of atrazine compared with hexazinone, DIA and 2,4-D. The enhanced oxidation kinetics of atrazine further resulted in the preferential oxidation of atrazine compared with 2,4-D, DIA and hexazinone, which contributed to the selective recognition ability to atrazine in PEC oxidation. Moreover, it was noted that without the electron-donating isopropyl group, the electron density of the triazine ring in DIA further decreased, which was not beneficial for the attacking of hydroxyl radicals, leading to lower PEC removal efficiency and slower oxidation kinetics. So finally, the selective removal ability of atrazine in complex water samples was investigated.

Here, real water sample was collected from Quyang sewage treatment plant in Shanghai to investigate the selective PEC oxidation performance of MI-meso-TiO₂ toward atrazine. COD of the water sample was detected as $30 \text{ mg}\cdot\text{L}^{-1}$. Then 2 ppm of atrazine was spiked. The prepared sample was to simulate the water in which atrazine was partially removed after conventional wastewater treatment. PEC oxidation on both meso-TiO₂ and MI-meso-TiO₂ was performed in order to clarify the selectivity. As shown in Fig. 7, a removal rate of 91.7% was obtained for atrazine on MI-meso-TiO₂, with a k_{app} of approximately 0.25 h^{-1} . However, the removal rate of atrazine on meso-TiO₂ was only

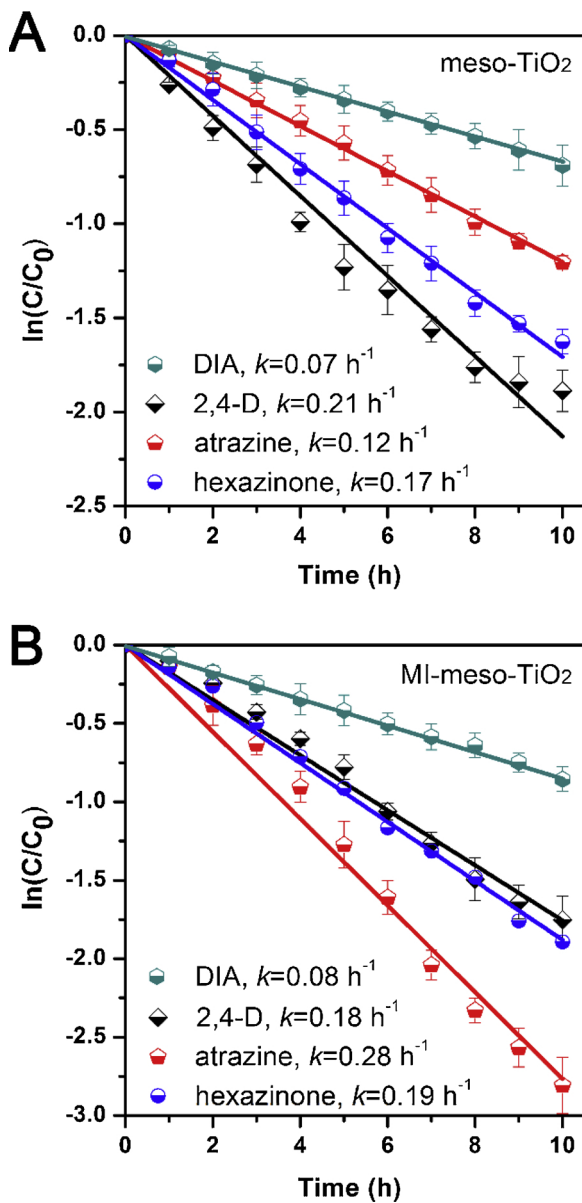


Fig. 6. PEC oxidation kinetics of atrazine, hexazinone, DIA and 2,4-D on (A) meso-TiO₂ and (B) MI-meso-TiO₂ in single component system.

57.2%, with a k_{app} of approximately 0.08 h^{-1} . We could observe that the oxidation of atrazine on meso-TiO₂ was evidently influenced by the coexistent organic matters in the water, whereas that was negligible on MI-meso-TiO₂. This result further confirmed the selective and enhanced PEC oxidation ability to atrazine, which was caused by the selective recognition ability of the MI sites on the photo-anode surface, and the preferential adsorption, binding and activation effect of MI-meso-TiO₂ towards atrazine.

3.4. The plausible PEC oxidation pathway of atrazine on MI-meso-TiO₂

In the work, the atrazine oxidation intermediates were also identified, and the results were listed in Table 2. Six main transformation products during the PEC oxidation of atrazine were found on both MI-meso-TiO₂ and meso-TiO₂, including hydroxylation products, de-alkylation products and oxidation products. These transformation products were similar with that identified in the reported literatures [38,39]. It suggested that the PEC oxidation pathway of atrazine was not influenced by introduction of MI sites, although the PEC oxidation efficiency

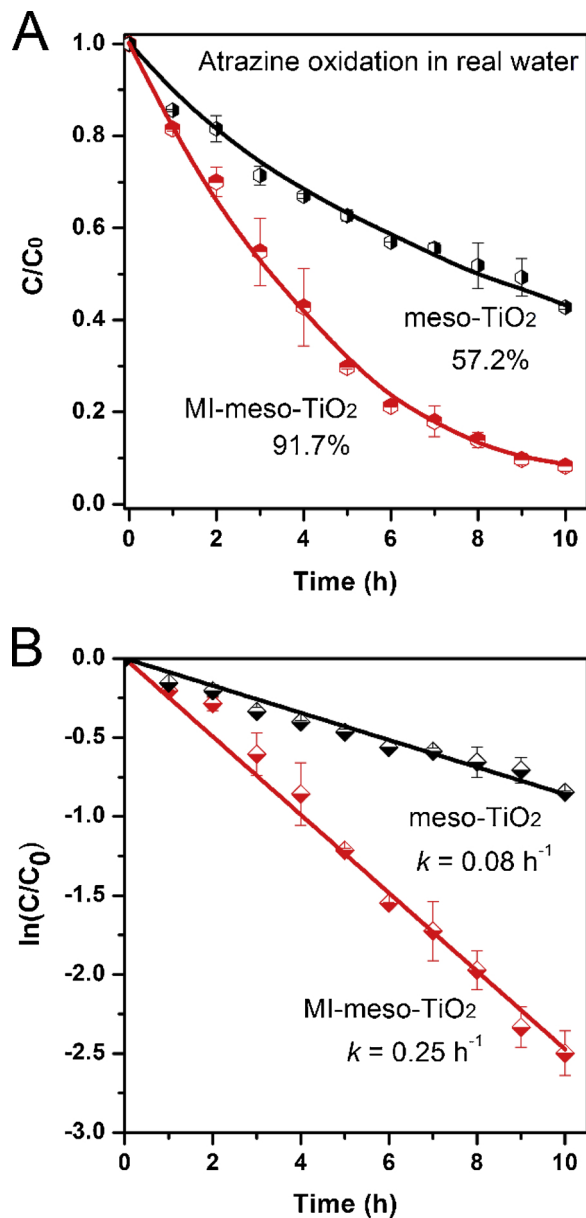


Fig. 7. Selective PEC oxidation of atrazine on MI-meso-TiO₂ in complex environmental water sample; the initial concentration of atrazine was 2 ppm.

was evidently improved. However, as shown in Fig. 8, there was some difference between MI-meso-TiO₂ and meso-TiO₂ concerning the rate of intermediates evolution and decay, which may be attributed to the introduction of the MI sites. We could find that there was a continuous accumulation of HA and DEHA on meso-TiO₂ in ten hours, while they were more rapidly accumulated and degraded on MI-meso-TiO₂. Additionally, we could observe that the concentration of HA and DEHA generated on MI-meso-TiO₂ was relatively larger than that on meso-TiO₂, whereas the concentration of DIA on MI-meso-TiO₂ was relatively smaller. It may indicate that hydroxylation products were more liable to be formed on MI-meso-TiO₂, and de-alkylation reaction occurred more easily on meso-TiO₂. Based on the detected degradation intermediates and the reported literatures [4,40], the oxidation pathway of atrazine was proposed and illustrated in Fig. S4.

The stability of MI-meso-TiO₂ in atrazine oxidation was also investigated from the perspective of actual application. The recycling capability of the MI-meso-TiO₂ was successfully evaluated by degrading atrazine over the reused photoanode. As shown in Fig. 9, the oxidation efficiency maintained at nearly the same level of the fresh samples after

Table 2

The major intermediates detected by means of LC/MS during PEC degradation of atrazine on MI-meso-TiO₂ and meso-TiO₂.

No.	Product	m/z	Molecular formula	Molecular structure
1	2-Hydroxy-4-ethylamino-6-isopropylamine-s-triazine(HA)	198	C ₈ H ₁₅ N ₅ O	
2	2-Chloro-4-amino-6-isopropylamine-s-triazine (DEA)	188	C ₆ H ₁₀ ClN ₅	
3	2-Chloro-4-ethylamino-6-amine-s-triazine (DIA)	174	C ₅ H ₈ ClN ₅	
4	2-Hydroxy-4-amino-6-isopropylamine-s-triazine (DEHA)	170	C ₆ H ₁₁ N ₅ O	
5	2-Chloro-4-acetamido-6-isopropylamine-s-triazine (CAIT)	230	C ₈ H ₁₂ ClN ₅ O	
6	N-(4-hydroxy-6-(isopropylamino)-1,3,5-triazin-2-yl)acetamide (HAIT)	212	C ₈ H ₁₃ N ₅ O ₂	

five consecutive runs for about 50 h. It suggested that the prepared MI-meso-TiO₂ exhibited good stability in atrazine oxidation, mainly attributed to the stable PEC catalytic ability of TiO₂, as well as the stable and excellent expression of the MI sites on TiO₂ surface with moderate rigidity.

4. Conclusions

In this work, MI-meso-TiO₂ was successfully fabricated with an EISA method combined with MI technique for enhanced and selective PEC oxidation of atrazine. The MI sites constructed on meso-TiO₂ could serve as surface defects which accelerated the holes transfer to the photo-anode surface and enhanced the generation of hydroxyl radicals. At the same time, MI sites embodied enhanced atrazine adsorption and PEC responses compared with that on bare meso-TiO₂, which resulted in the improved PEC oxidation of atrazine on MI-meso-TiO₂. The binding behavior of atrazine on MI-meso-TiO₂ was also investigated by in situ ATR-IR and UV-vis DRS spectra, indicating formation of synergic hydrogen bonding and halogen bonding etc., which also played more efficient activation role to atrazine adsorbed on MI-meso-TiO₂ in PEC oxidation process compared to meso-TiO₂. Meanwhile, the selective recognition ability of MI-meso-TiO₂ toward atrazine was also investigated based on the selective and improved adsorption of atrazine compared with 2,4-D and hexazinone, as well as the selective enhancement of PEC atrazine oxidation efficiency. Finally, selective PEC removal of atrazine in practical waste water was also performed, and the results indicated that the co-existent interferences didn't influence the removal rate and oxidation kinetics of atrazine on MI-meso-TiO₂, whereas the influence on meso-TiO₂ was more evident. The present work suggested that selective PEC oxidation based on MI technique was a promising method to be integrated with traditional water treatment methods for deep treatment of specific pollutant with high selectivity from the viewpoint of efficiency and cost-effectiveness.

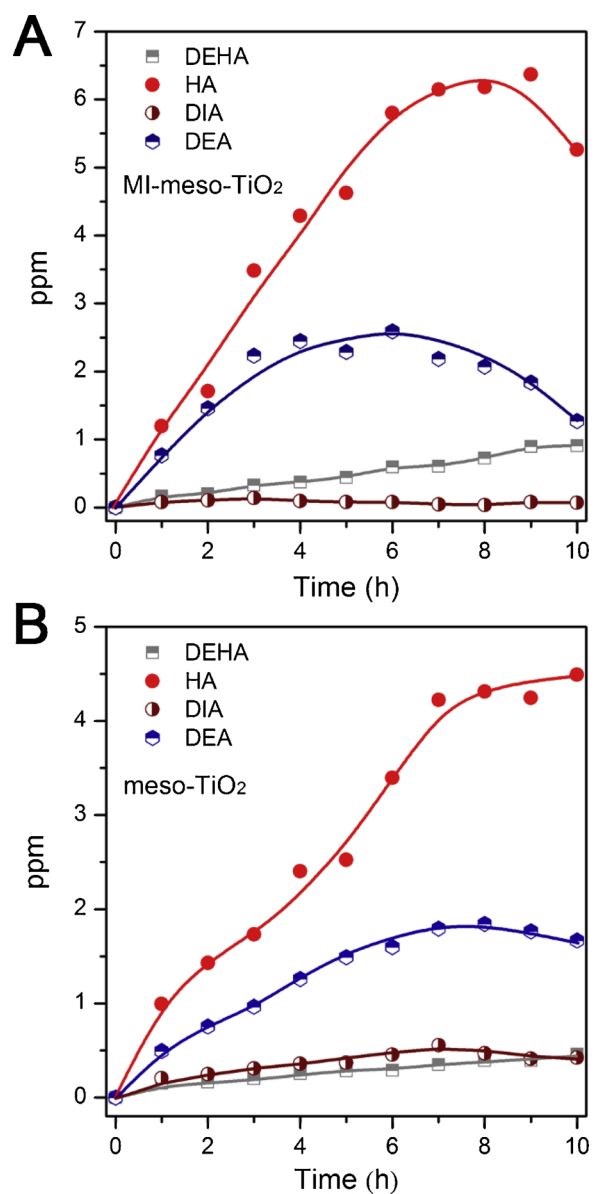


Fig. 8. Evolution and decay of the degradation intermediates determined by HPLC.

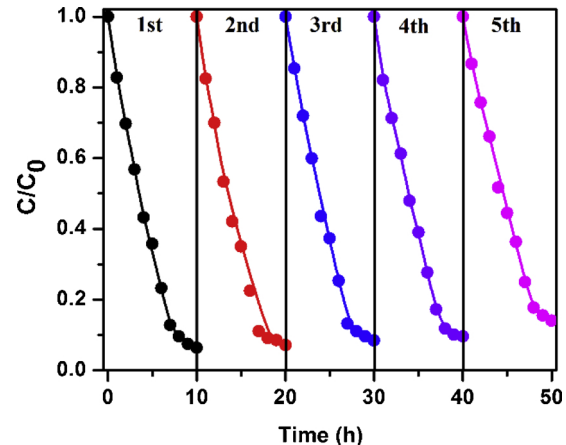


Fig. 9. Stability of MI-meso-TiO₂ in PEC oxidation of atrazine.

Acknowledgments

We acknowledge funding from the National Natural Science Foundation of China (Project No. 21677110, 21537003 and 21777115). Also, the work is supported by the Science & Technology Commission of Shanghai Municipality (14DZ2261100), the Fundamental Research Funds for the Central Universities (22120180118) and the State Key Laboratory of Pollution Control and Resource Reuse Foundation (NO. PCRRF17013).

Appendix A. Supplementary data

Supplementary material related to this article can be found, in the online version, at doi:<https://doi.org/10.1016/j.apcatb.2019.01.018>.

References

- [1] J. Romao, G. Mul, ACS Catal. 6 (2016) 1254–1262.
- [2] K. Schouteten, T. Hennebel, E. Dheere, C. Bertelkamp, D.J. De Ridder, S. Maes, M. Chys, S.W.H. Van Hulle, J.V. Bussche, L. Vanhaecke, A.R.D. Verliefde, Chemosphere 165 (2016) 191–201.
- [3] M.S. Koo, K. Cho, J. Yoon, W. Choi, Environ. Sci. Technol. 51 (2017) 6590–6598.
- [4] S. Komtchou, A. Dirany, P. Drogui, N. Delegan, M.A. El Khakani, D. Robert, P. Lafrance, Chemosphere 157 (2016) 79–88.
- [5] Y.N. Zhang, N. Qin, J. Li, S. Han, P. Li, G. Zhao, Appl. Catal. B 216 (2017) 30–40.
- [6] G. Li, Z. Lian, W. Wang, D. Zhang, H. Li, Nano Energy 19 (2016) 446–454.
- [7] L. Wu, F. Li, Y. Xu, J.W. Zhang, D. Zhang, G. Li, H. Li, Appl. Catal. B 164 (2015) 217–224.
- [8] H.J. Shi, C. Chen, B. Tang, G.H. Zhao, Electrochim. Acta 146 (2014) 359–364.
- [9] L. Chen, X. Wang, W. Lu, X. Wu, J. Li, Chem. Soc. Rev. 45 (2016) 2137–2211.
- [10] Y.N. Zhang, W.G. Dai, Y.Z. Wen, G. Zhao, Appl. Catal. B 212 (2017) 185–192.
- [11] C. Chen, H.J. Shi, G.H. Zhao, J. Phys. Chem. C 118 (2014) 12041–12049.
- [12] C.C. de Escobar, M.A. Lansarin, J.H.Z. dos Santos, J. Hazard. Mater. 306 (2016) 359–366.
- [13] X.B. Luo, F. Deng, L.J. Min, S.L. Luo, B. Guo, G.S. Zeng, C.T. Au, Environ. Sci. Technol. 47 (2013) 7404–7412.
- [14] S.N. Chai, G.H. Zhao, Y.N. Zhang, Y.J. Wang, F.Q. Nong, M.F. Li, D.M. Li, Environ. Sci. Technol. 46 (2012) 10182–10190.
- [15] W. Zhou, W. Li, J.Q. Wang, Y. Qu, Y. Yang, Y. Xie, K. Zhang, L. Wang, H. Fu, D. Zhao, J. Am. Chem. Soc. 136 (2014) 9280–9283.
- [16] W. Li, Z. Wu, J. Wang, A.A. Elzatahry, D. Zhao, Chem. Mater. 26 (2014) 287–298.
- [17] C. Wattanakit, Y.B. Come, V. Lapeyre, P.A. Bopp, M. Heim, S. Yadnum, S. Nokbin, C. Warakulwit, J. Limtrakul, A. Kuhn, Nat. Commun. 5 (2014) 3325–3332.
- [18] J.X. Yang, J. Li, W.Y. Dong, J. Ma, J. Cao, T.T. Li, J.Y. Li, J. Gu, P.X. Liu, J. Hazard. Mater. 316 (2016) 110–121.
- [19] W.-K. Wang, J.-J. Chen, M. Gao, Y.-X. Huang, X. Zhang, H.-Q. Yu, Appl. Catal. B 195 (2016) 69–76.
- [20] N. Bensalah, S. Dbira, A. Bedoui, J. Environ. Sci. 45 (2016) 115–123.
- [21] A.Y. Zhang, W.K. Wang, D.N. Pei, H.Q. Yu, Water Res. 92 (2016) 78–86.
- [22] L. Wang, M.H. Cao, Z.H. Ai, L.Z. Zhang, Environ. Sci. Technol. 49 (2015) 3032–3039.
- [23] J.Q. Fan, H.J. Shi, H. Xiao, G.H. Zhao, ACS Appl. Mater. Interfaces 8 (2016) 28306–28315.
- [24] X. Zhao, D. Pan, X. Chen, R. Li, T. Jiang, W. Wang, G. Li, D.Y.C. Leung, Appl. Catal. B 467–468 (2019) 658–665.
- [25] W.-K. Wang, M. Gao, X. Zhang, M. Fujitsuka, T. Majima, H.-Q. Yu, Appl. Catal. B 205 (2017) 165–172.
- [26] J. Farmer Budarz, A. Turolla, A.F. Piasecki, J.Y. Bottero, M. Antonelli, M.R. Wiesner, Langmuir 33 (2017) 2770–2779.
- [27] T.E. Chien, K.L. Li, P.Y. Lin, J.L. Lin, Langmuir 32 (2016) 5306–5313.
- [28] E. Benassi, M. Di Foggia, S. Bonora, Comput. Theor. Chem. 1013 (2013) 85–91.
- [29] A. Dutta, A. Mandal, S. Manna, S.B. Singh, A.E. Berns, N. Singh, Environ. Monit. Assess. 187 (2015) 620–631.
- [30] X. Zhang, X. Ke, Z. Zheng, H. Liu, H. Zhu, Appl. Catal. B 150–151 (2014) 330–337.
- [31] J. Dai, J. Yang, X.H. Wang, L. Zhang, Y.J. Li, Appl. Surf. Sci. 349 (2015) 343–352.
- [32] X.T. Shen, L.H. Zhu, N. Wang, T. Zhang, H.Q. Tang, Catal. Today 225 (2014) 164–170.
- [33] J. Zeng, Q. Zhang, J. Chen, Y. Xia, Nano Lett. 10 (2010) 30–35.
- [34] M. Humayun, Y. Qu, F. Raziq, R. Yan, Z. Li, X. Zhang, L. Jing, Environ. Sci. Technol. 50 (2016) 13600–13610.
- [35] C. Sun, S.A. Baig, Z. Lou, J. Zhu, Z. Wang, X. Li, J. Wu, Y. Zhang, X. Xu, Appl. Catal. B 158–159 (2014) 38–47.
- [36] S. Chai, Y. Wang, Y.N. Zhang, M. Liu, Y. Wang, G. Zhao, Environ. Sci. Technol. 51 (2017) 8067–8076.
- [37] A. Kapalka, G. Foti, C. Comninellis, Electrochim. Acta 54 (2009) 2018–2023.
- [38] H. Yang, H.Q. Wei, L.T. Hu, H.J. Liu, L.P. Yang, C.T. Au, B. Yi, Chem. Eng. J. 300 (2016) 209–216.
- [39] W.K. Jo, J.Y. Lee, N.C.S. Selvam, Chem. Eng. J. 289 (2016) 306–318.
- [40] E.M. Samsudin, S.B. Abd Hamid, J.C. Juan, W.J. Basirun, G. Centi, Chem. Eng. J. 280 (2015) 330–343.